MTLA 30 (2023) 101856

Contents lists available at ScienceDirect

Materialia

journal homepage: www.elsevier.com/locate/mtla

The development of ultrafine grain structure in an additively manufactured titanium alloy via high-temperature microscopy

Marco Simonelli [a,*], Zhiyi Zou [a], Pere Barriobero-Vila [b], Yau Yau Tse [c]

[a] Centre for Additive Manufacturing, Faculty of Engineering, University of Nottingham, Nottingham NG8 1BB, United Kingdom
[b] Technical University of Catalonia (UPC), Department of Materials Science and Engineering, Eduard Maristany Av. 16, 08019 Barcelona, Spain
[c] Department of Materials, Loughborough University, Loughborough LE11 3TU, United Kingdom

ARTICLE INFO

Keywords:
Additive manufacturing
Laser powder-bed fusion
Ti alloys
Ti-6Al-4V

ABSTRACT

Microstructures dominated by acicular α' martensitic phase, such as in the case of Ti-6Al-4V fabricated by laser powder-bed fusion (PBF-LB), are known to suffer from reduced ductility and low toughness. The decomposition of such metastable microstructures into α+β lamellar structures during PBF-LB requires either specific laser regimes that are often challenging to be attained or post-process heat treatments which might lead, instead, to undesirable coarsening of the grain structure. Here we propose a novel route for the formation of ultrafine lamellar α+β microstructures and demonstrate the associated advantages in terms of tensile strength and ductility. Our approach is based on a suitable modification of constitution of Ti-6Al-4V with additions of Fe, a known potent β stabiliser of high intrinsic diffusivity. After printing, this alloy presents a microstructure dominated by metastable β phase. We investigate the details of its decomposition using a combination of in-situ high-energy synchrotron X-ray diffraction and high temperature microscopy up to the β transus temperature. The microstructure evolution is comprised by homogeneous decomposition of the metastable β phase via ω-assisted nucleation of α phase, α grain growth sustained by early diffusion of Fe in the β phase followed by a conventional partitioning of V. The understanding of this transformation pathway enables the development of ultrafine grained α+β lamellar microstructures that exhibit outstanding tensile behaviour. The presented approach is machine-agnostic and offers a novel alloy design strategy for development of high-strength alloys in additive manufacturing.

1. Introduction

The use of Laser Beam Powder Bed Fusion (PBF-LB) to manufacture Titanium (Ti) alloys, and in particular Ti-6Al-4V, has the potential to open up new applications in the medical and aerospace sectors. As PBF-LB is a net-shape manufacturing technique, and no mechanical post-processing is permissible, most of the research conducted in this field, has focused on the relationship between process parameter (and the associated thermal profiles) and the development of acceptable microstructures capable to reach desirable mechanical properties [1]. It is in fact known that a range of different α/β phase fractions and grain morphologies can be obtained by manipulating the laser process parameters or via post-process heat treatments, thus resulting in a variety of strength and ductility combinations. Out of this body of literature, the generation of *ultrafine* lamellar (α+β) structures (average α lath thickness smaller than 1 μm [2]) has sparked particular interest in the community as these structures are associated to excellent strength and ductility. With the attainment of ultrafine lamellar microstructure being the goal of our work, we present here the microstructural evolution of a newly developed quaternary Ti alloy via PBF-LB and subsequent heat treatment.

Owing to the highly localised melting and solidification events during PBF-LB, rapid heating and cooling cycles through the β transus and martensitic start M_s temperatures of (α+β) Ti alloys limit any diffusion-controlled microstructural transformations [3,4]. The PBF-LB process is thus naturally conducive to the formation of fine microstructures. However, considering Ti-6Al-4V as an example of the typical PBF-LB response of (α+β) Ti alloys, hierarchical α′ martensites [5] coexisting with nanometric thin (often undetected) β ribs [6,7] within vertically oriented prior-β grains, describe a ubiquitous microstructural signature. The width of the α'martensite (and residual β ribs morphology) seems to be influenced by varying laser power, laser speed

* Corresponding author.
E-mail address: Marco.Simonelli@nottingham.ac.uk (M. Simonelli).

https://doi.org/10.1016/j.mtla.2023.101856
Received 15 May 2023; Accepted 20 July 2023
Available online 21 July 2023

and laser scan strategy as these process variables intrinsically affect the cooling rates experienced by the material during the $\beta \leftrightarrow \alpha'$ cyclic transformations that take place during deposition [4,7]). Nevertheless microstructures where martensite and retained β coexisting are associated to reduced ductility (typical elongation to failure of 5 ± 1%) and should be avoided for structural applications.

Prior studies, including the seminal work by Kelly and Kampe [8], have then focused on using the intrinsic thermal cycle associated to additive manufacture to promote α′ martensite decomposition [6,7, 9-11]. It is established that a fundamental requirement for *in-situ* dissolution of α' martensite is to expose the material to temperatures where diffusion kinetics are significant to enable the partitioning of β-stabilisers into the β phase. Considering the repeating thermal cycles that characterise laser-based AM, it is also thought that dissolution of metastable phases could take place when laser parameters are chosen to reduce the cooling rates through the M_s temperature, with a net cumulate effect of extending residence times at temperatures where diffusional transformations may take place [12]. The difficulty to reliably experimentally measure the thermal history experience by the layers and the lack of high-fidelity models that at part scale make it had to rationalise the exact kinetics of martensitic decomposition. Often studies refer to volumetric energy density as a broad brush parameter to estimate whether decomposition of martensite might take place during the process [6,12]. Using a combination of modelling and microstructural investigations, some studies have indicated that *in situ* martensitic decomposition in Ti-6Al-4V might take place in layers where temperatures are as high as 650 to 800 °C [9,11]: this clearly far exceeds the quasi-static temperature (~ 400 °C) for which decomposition of martensite is generally started to be visible as the rapid heating and cooling cycles rates between β transus temperature and M_s characteristic of PBF-LB - estimated between 10^4 and $10^{6\circ}$C/s (depending on the relative distance from the processing plane) [13] - produce very short residence times where diffusion takes place [7]. In fact, there are reports that show that even 6 h at 800 °C are not complete for a decomposition of α' in PBF-LB of Ti-6Al-4V [14]. It is thus conceivable that in most manufacturing conditions, there will be always regions of the build where the metastable phase (e.g. α′ martensite) decomposition is incomplete [11,15]. Additionally, specific processing pathways that might encourage decomposition of α' (e.g. heated substrates, scan strategy, laser spot size, layer thickness etc.) might not be reproducible when different additive platforms are used or at a component-scale where complex geometries lead to inevitable temperature profile deviations and spatial microstructure variations [16]. For these reasons, *in situ* decomposition of metastable phases during PBF-LB (and more generally AM) remains fundamentally based on based on trial and error approach and is difficult to implement at an industrial level.

Research has also shown how post-process heat treatments can be useful to recover or anneal microstructures of the printed components [17] and are considered inevitable to eliminate residual stresses imparted by PBF-LB. However, the annealing temperatures required to fully decompose metastable microstructure (T ~ 800°C or higher in the case of the martensitic structure of Ti-6Al-4V for example [9]) lead to coarsening of α laths resulting in a typical penalty in strength (as per Hall-Petch type relationship) [12,18]. As the decomposition of metastable microstructures resulting from AM is strictly dependent on the diffusional kinetics characteristic of the alloy, suitable design of the alloy constitution might enable the decomposition of α' at lower temperatures (thus avoid coarsening) thus leading to the development of ultrafine α+β structures.

To test this hypothesis, we study the influence of Fe on the microstructure development of Ti-6Al-4V during PBF-LB and a subsequent heat treatment. Prior work [19,20] demonstrates that the intrinsic fast solidification and cooling rate occurring during laser-based additive manufacture, enable processing of Ti compositions rich in β-eutectoid formers (e.g. Fe) without typical segregation defects (i.e. β-flecks) that would otherwise typically occur during ingot manufacture. Additionally, moderate additions of Fe (e.g. 3 wt.%) are known to have a profound impact on the nature of the metastable phases that result from rapid solidification, which in turn are thought to provide a flexible response to heat treatment [19,21]. Using a combination of *in-situ* HEXRD, high-temperature microscopy and thermodynamic calculations, this paper elucidates the formation of metastable phases in a quaternary alloy obtained from PBF-LB of a Ti-6Al-4V + 3Fe (wt.%) powder mixture and delineates a metallurgical route to achieve ultrafine α+β microstructures following heat treatment.

2. Experimental procedures

2.1. Manufacturing of specimens: laser powder-bed fusion and heat treatments

The materials used in this study are (i) pre-alloyed plasma atomised ELI Ti-6Al-4V (reference material) and (ii) a novel quaternary Ti-6Al-4V + 3Fe (wt.%) powder mixture (for simplicity, hereafter indicated asTi-6Al-4V-3Fe). The reference material was supplied from Carpenter AM and consisted of spherical plasma atomised powders with size distribution D10 = 22.1 μm, D50 = 33.5 μm, and D90 = 49.9 μm. The Ti-6Al-4V-3Fe was obtained by adding ELI Ti-6Al-4V with 99.9 pct pure Fe particles (GoodFellow Cambridge Limited) of size distribution D10 = 2.9 μm, D50 = 5.7 μm, and D90 = 12.7 μm. To reach the desired composition, every 97g of Ti-6Al-4V were mixed with 3g of Fe. Prior to the PBF-LB printing process, both reference and mixed feedstock powders were dried overnight at 70°C to minimise moisture content.

The two powder feedstocks were processed using a Renishaw AM400 PBF-LB platform. The AM400 platform was operated using the laser parameters listed in Table 1 to achieve near-fully dense components (density > 99.8%). Each layer was melted once using a continuous fibre laser (1070 nm), which is modulated in power. The laser achieves a pulsed output defined by a pulse length (i.e. exposure time) and point distance (distance between pulse exposures) – Table 1. The specimens were manufactured at focus (focal offset distance equal to zero), where the laser measures a nominal 70 spot diameter. The laser scan direction was then rotated by 67 degrees between two consecutive layers to randomise the average scan vector lengths per cross-section. To facilitate powder spreading during the build cycle, the AM400 build platform was kept at 170°C during operation. The process chamber atmosphere was regulated with circulating Ar to keep oxygen levels below 0.04 pct.

The specimens investigated were produced across four consecutive builds. The test geometries are cubes of 10 mm and cylinders (60 mm height and 9 mm diameter) built in the horizontal orientations (as per ASTM E8/E8M- 16a [22]). Tensile testing is carried out after heat treatments in Ar protective atmosphere with an average heating and cooling rate of 10°C/min, a dwell time of 2 hours and a soaking temperature of 730°C.

2.2. Microstructural evolution: room and high temperature microscopy combined with in situ high-energy synchrotron X-ray diffraction

For the sake of clarity, the microstructures presented in this study are obtained from examinations of the frontal plane of the specimens, which is parallel to the PBF-LB building direction. This is consistent with the majority of the literature on microstructural development during PBF-LB.

The room temperature microstructure was investigated using a range of techniques, including backscatter imaging and energy-dispersive spectroscopy (EDS) on a JSM-7800F FEG-SEM using an accelerating voltage of 20kV, aperture 4, probe current 16mA and a working distance of 20 and 10mm respectively. The average thickness of the microstructural features (α/β lath) was measured from backscattered electron microscopy images via modified mean linear intercept methods, as recommended by Vander Voort and Roósz [23].

The microstructure evolution as a function of temperature was

Table 1
PBF-LB process parameters used to manufacture the studied Ti-6Al-4V and Ti-6Al-4V-3Fe alloys investigated in this study.

Power (W)	Exposure time (μs)	Inter-point delay (μs)	Point distance (μm)	Hatch spacing (μm)	Layer thickness (μm)	Volumetric energy density (J/mm^3)
195	50	20	75	65	30	66.67

investigated *in situ* by high temperature microscopy and in situ high-energy synchrotron X-ray diffraction (HEXRD). For high temperature microscopy, thin plates (approx. dimensions of 3 × 3 × 1mm) were extracted from as-built specimens and prepared using standard metallurgical procedures [19,24]. The polished thin plates were then installed on a heating SEM stage (Murano in-situ stages, Gatan) using high temperature carbon paste to allow for a controlled and progressive heating of the specimens (up to 950°C) and simultaneous SEM imaging. Imaging was carried out on a JEOL 7100F FEG-SEM using an accelerating voltage of 15kV, aperture 2, probe current 12mA, and a fixed working distance of 20mm. For temperatures below 700°C, the images are taken using the forescatter (FS) detectors to generate electron channelling contrast. Since higher temperatures saturated the FS detectors, the images were taken in this case by detecting secondary electrons. During the investigation, stage temperature was monitored via a spot-welded thermocouple embedded underneath the sample plate. The temperature was increased in 30°C steps with dwell times of 15 minutes or more to achieve uniform degassing and temperature distribution. High temperature EBSD was also carried out at selected temperatures (720, 750, 790, 840 and 890°C) using a step size of 0.1 μm. The collected data was analysed using HKL-Channel 5 ^{TM} and mapped in Z-IPF. Room temperature EBSD was carried out using a step size of 0.4 μm of the frontal planes of Ti-6Al-4V and Ti-6Al-4V-3Fe. Transmission electron microscopy (TEM), scanning transmission electron microscopy (STEM) and SETM-EDX were performed on Tecnai F20 operated at 200kV.

In situ HEXRD was carried out at the P07-HEMS beamline of PETRA III (Deutsches Elektronen-Synchrotron) as described in detail in [25]. The phase transformation kinetics of the material in the PBF-LB as-built condition was investigated during continuous heating at 100°C/min from room temperature up to 900°C (*i.e.*, up to a temperature close to the β transus of the Ti-6Al-4V-3Fe alloy). An energy of 100 keV (λ = 0.0124 nm) was used. The acquisition time and sample-detector distance were 5 seconds and 1926 mm, respectively. The investigated samples were cut from the centre of as-built SLM cubes and were investigated close to the centre of the building height in transmission mode using a gauge volume of 0.8 × 0.8 × 5 mm^3. The temperature was controlled by a spot-welded thermocouple located next to the position of the incident beam. Qualitative analysis of the evolution of the diffraction patterns was carried out by converting the Debye–Scherrer rings into Cartesian coordinates (Azimuthal angle ψ, 2θ). Subsequently, projection of the summed intensity of Bragg reflections on the 2θ axis was performed using the software ImageJ. The instrumental parameters of the HEXRD setup were obtained using a LaB_6 powder standard. Quantitative analysis of volume fraction of phases was determined by the Rietveld method as implemented in the software Maud [26].

2.3. Equilibrium thermodynamic calculations

The equilibrium phase diagrams for Ti-6Al-4V and Ti-6Al-4V-3Fe were evaluated using ThermoCalc and the commercially available Ti-database TCTi2. In the case of Ti-6Al-4V, phase diagrams were experimentally validated using literature [27–29]. High temperature EBSD and HEXRD were instead used to validate the calculations on Ti-6Al-4V-3Fe. Where needed, the elemental concentration (wt. %) in the α and β phases of the two alloys was calculated by dividing the mass of the element of interest in the alloy divided by the predicted phase fraction amounts at each computed temperature.

2.4. Tensile characterisation

Tensile specimens with a diameter of 4 mm and a gauge length of 20.4 mm were machined from the centre of the PBF-LB printed cylinders, according to standard ASTM E8/E8M- 16a [22]. Tensile tests were then conducted at room temperature on an Instron 5969 at a strain rate of 0.14 mm/min. Specimens were tested perpendicular to the build-direction of the cylinders.

3. Results

3.1. Microstructural features in the as-built condition of Ti-6Al-4V-3Fe

To understand the influence of Fe on the microstructure evolution during PBF-LB it is useful to contrast micrographs obtained from the two materials under identical processing conditions. Ti-6Al-4V specimens (Fig. 1a) present a martensitic microstructure where no residual β phase is detected by SEM (as is the case in most of the literature) [11,22,23].

Acicular α′ martensite is distributed within elongated prior β grains which develop across several layer depositions. The martensitic transformation hinders the visualization of melt pool boundaries resulting from PBF-LB. As shown in Fig. 1b, the as-built microstructure of Ti-6Al-4V-3Fe consists predominantly of two phases, namely α′ martensite and metastable β, as reported in our prior research [19]. The β grains present a predominant vertical elongation spanning across different melt pools along the build direction, signalling the occurrence of epitaxial growth. Noteworthy is also the discernible presence of grain boundary α at certain β grain boundaries and the melt pool boundaries arcs (both these features are generally not visible in Ti-6Al-4V). Solidification dendrites are not visible, most likely due to the presence of the fine α′ structures, which replaces the common dendritic structures observed in other cubic systems processed by PBF-LB [30]. Mixed powder feedstocks lead to variations of Fe across different build locations and it is observed that phase fractions and arrangement relates to the distribution of Fe in the build (Supplementary Figure S1). The vast majority of the microstructure of Ti-6Al-4V-3Fe consists of β grains with Fe concentrations of 2.5 ± 0.5 wt.%. For clarity, these grains will be denoted as β^L in the rest of this manuscript. The interior of these β grains presents fine α′ precipitates that appear as faint microstructural features in SEM but become clearly discernible under TEM observation (Fig. 2a). Coexisting with α′ precipitates, athermal ω phase is detected in the β matrix, appearing with distinctive streaky reflections in the diffraction patterns in Fig. 2a.

Table 2 shows the results of EDS point analysis performed on the phase constituents appearing in Fig. 2 while elemental maps are shown in Fig. 3. The analysis shows that no significant elemental difference between athermal ω phase and β matrix due to the detection and resolution limit of the STEM-EDS. The fine α′ presents a lower concentration of Fe with respect to the surrounding β matrix, as shown in Fig. 3 and Table 2. However, the results reveal no significant chemical compositional difference in Al and V between the β grains and fine α′ precipitates within the spatial resolution of nm range. This evidence indicates that fast heating and cooling associated with the PBF-LB processing cause, overall, limited elemental partitioning between the α′ and β matrix (Table 2).

In addition to β^L grains, the as-built microstructure presents localised iron-poor regions, with Fe concentration only reaching 0.5% ± 0.1%. These areas are dominated by α′ martensites phase, clearly resembling the microstructure of as-printed Ti-6Al-4V. Finally, iron-rich regions with no apparent α′ martensite are also observed, with a typical Fe concentration exceeding 3.5 wt.%. These regions will be denoted as β^H.

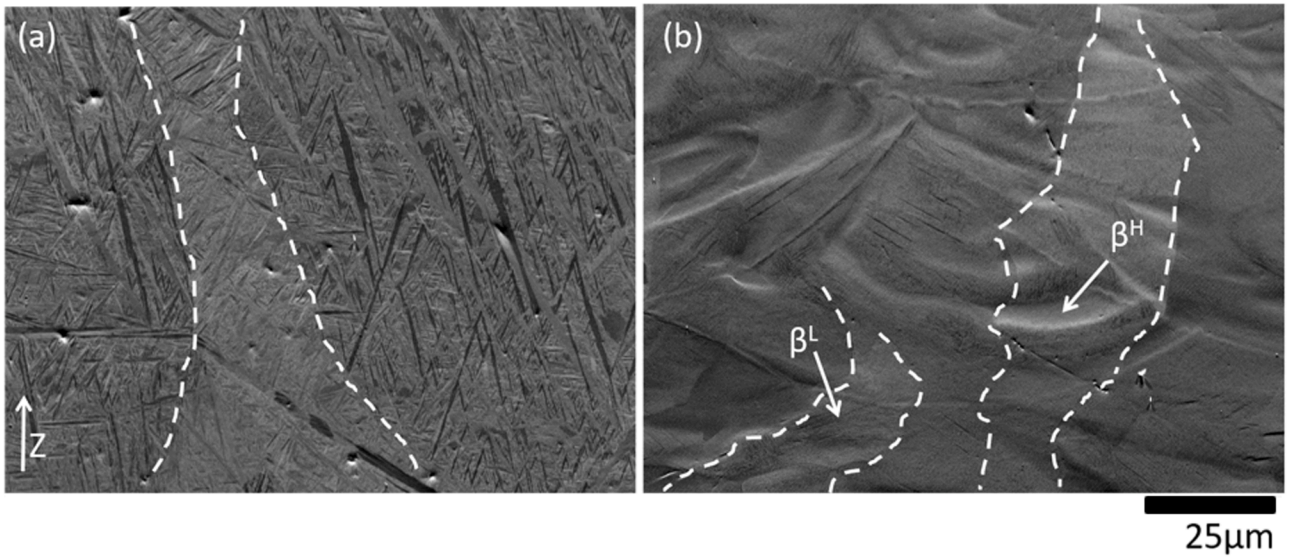

Fig. 1. SEM-BSE images of the as-built PBF-LB microstructures of the (a) Ti-6Al-4V and (b) Ti-6Al-4V-3Fe alloys. Some of the prior-β grain boundaries are highlighted using white dashed lines. The build direction is also indicated in the figure using a white arrow. β grains with moderate and high concentration of Fe (β^L and β^H) are indicated in (b).

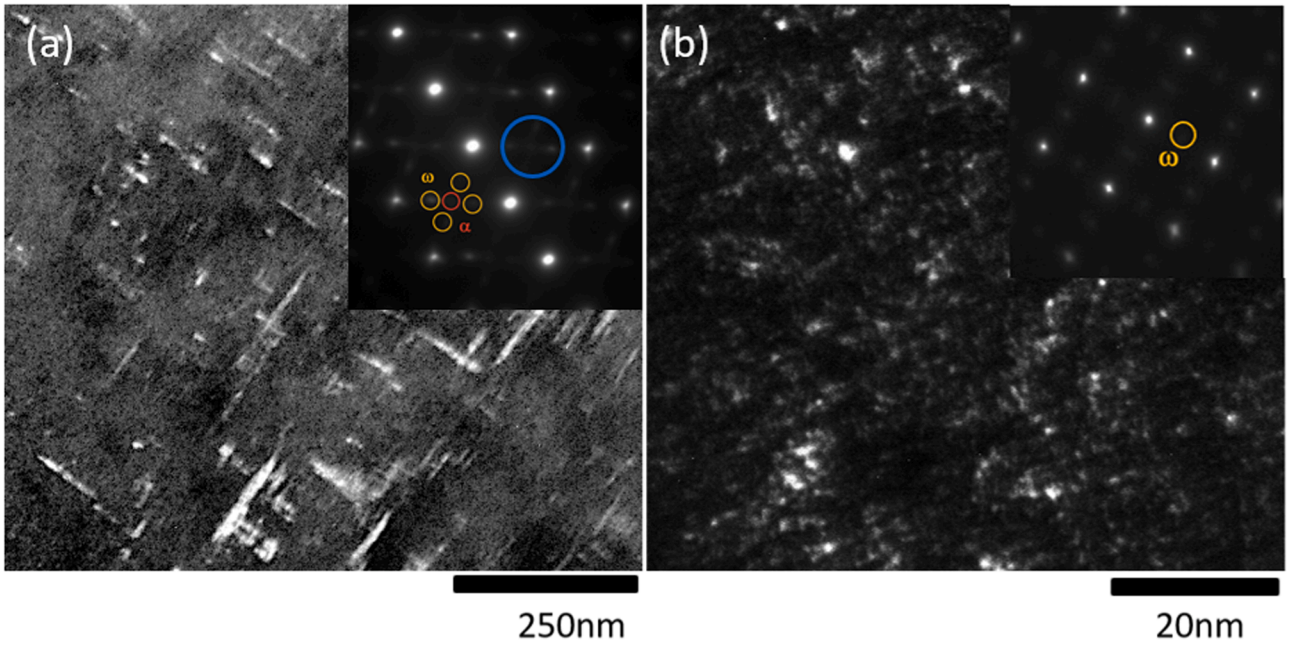

Fig. 2. Fine structure inside metastable β grains in Ti-6Al-4V-3Fe after PBF-LB. (a) Dark-field TEM image and the selective area diffraction pattern (insert) along the [110]β zone axis, showing fine α′ lath and athermal ω in the β matrix. (b) Dark-field micrograph and selective area diffraction pattern (insert) revealing the fine dispersion of ω phases under [001]β zone axis. The dark-field diffraction contrast of the ω phases is obtained using the $[\bar{2}1\bar{1}]$ reflection marked by the blue circle in [110] β diffraction pattern as shown in the inset of (a).

Table 2
Composition of Ti-6Al-4V-3Fe in the as-built condition measured by TEM-EDS.

Microstructural Feature	Element (Wt Pct)			
	Ti	Al	V	Fe
β matrix	bal.	6.0 ± 0.2	3.8 ± 0.3	2.9 ± 0.1
fine α′ in β matrix	bal.	6.2 ± 0.2	3.3 ± 0.3	2.0 ± 0.1
Isolated α′ martensite	bal.	6.5 ± 0.2	3.9 ± 0.1	0.5 ± 0.1

3.2. Microstructural evolution under rapid and near-equilibrium thermal treatment

The analysis of *in situ* HEXRD presented Fig. 4 allows to study the overall bulk phase transformation kinetics during continuous heating of the metastable β phase obtained within the as-built PBF-LB Ti-6Al-4V-3Fe. At room temperature, the metastable β accounts for 70 vol.% of the microstructure. During heating up to 400°C, no significant diffusion takes place as indicated by no overall changes in peak intensity or position. As the temperature increases, in the range of 400°C to 700°C, a decrease in the volume fraction of β from 70 vol.% to 25 vol.% is

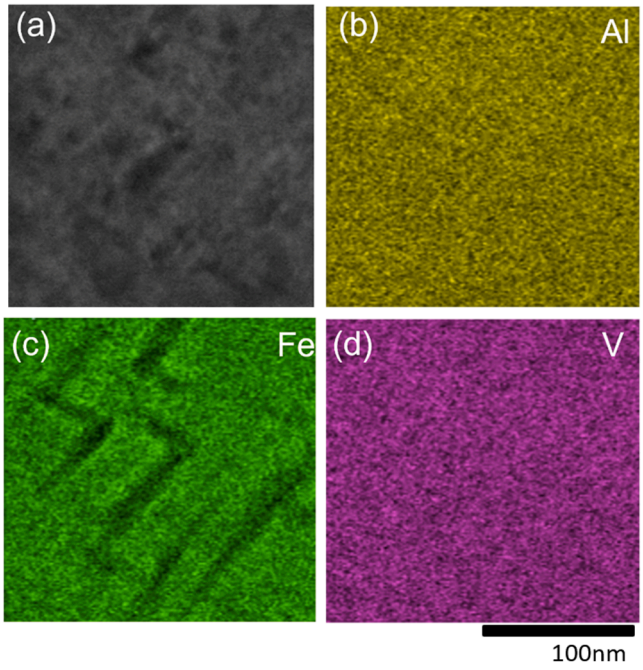

Fig. 3. Compositional differences in the fine structure inside metastable β grains in Ti-6Al-4V-3Fe after PBF-LB. (a) STEM Bright field TEM image showing the dominant beta matrix and fine α′ lath. (b), (c), (d) corresponding STEM-EDX maps showing the distribution of aluminium, iron and vanadium, respectively.

observed (Fig. 4b). This indicates that metastable β is progressively transforming to α phase during this stage of the heating. This transformation is associated with solute partitioning, as reflected in the shift of the peak positions. For instance, it is observed that the $\{200\}_{\beta}$ reflection shifts to higher 2θ between 400 and 650°C with respect to the initial condition, suggesting an associated contraction in the lattice parameter. It is noteworthy that during this temperature range, no shifts occur in Ti-6Al-4V [7]. The associated contraction in lattice parameter is likely due to the progressive Fe enrichment in the β phase, caused by a combined effect of Fe rejection into the β phase [31] during α formation and a progressive decrease in the weight fraction of total β phase (leading to higher Fe concentrations in the retained β phase). The $\{200\}_{\beta}$ reflection shifts then to lower 2θ between 650°C up to the β transus temperature (estimated close to 900°C). For temperatures above 700°C, a further phase transformation is enabled, with α transforming to β phase as expected from the equilibrium phase relationships. Moreover, during this stage of the heating we observe a progressive shift of the {110}β, {200}β and {211}β reflections towards lower 2θ corresponding to an expansion of the lattice parameter of the β phase. This is attributed to a progressive increase of the volume fraction of beta and enrichment of this phase in elements such as V and Ti, respectively [7,32]. As temperature reaches 900°C, the microstructure consists of approximately 40% of the β phase. On the other hand, after a 30-minute dwell at 900°C, the structure consists almost exclusively of β phase (Fig. 4 (b)).

High-temperature microscopy is then used to determine the evolution of the microstructure at a microscale and investigate the influence of Fe on the kinetics of the phase transformation. Fig. 5a shows a region of interest with metastable β grains with relatively low and high Fe concentration (indicated as β^{L} and βH, respectively, in section 3.1 and marked by green and orange) and portions of microstructure dominated by fine α′ martensite (white stars). Following the progress from Fig. 5a-c, it is observed that β^{H} regions are the first locations of the microstructure to transform as the temperature is increased. At room temperature these regions of the microstructure possess distinct lack of surface topography or any α′ phase contrast. It can be noticed that their transformation, which is visible due to the changes in the surface topography, is triggered at temperatures as low as ~300°C (Fig. 5c). EBSD phase analysis indicates that the new phase that forms in these areas has a HCP symmetry. The extent of this transformation is however minimal. This transformation is either not detected by HEXRD or is retarded to 350-400°C as a consequence of the continuous rapid heating (100°C/min) used in the HEXRD experiments. The α grain structure in these areas becomes well defined at temperatures equal or higher than 400°C (Fig. 5d). At this temperature it possible to resolve some α_{GB} as these delineate β grains (indicated by red arrows) although the majority of α/α′structures remain too fine to be fully characterised. It is noted that most of the β structure is consumed by the α phase when temperature is raised up to 500°C (Fig. 5e-f). For temperatures ranging from 500 to 700°C (Fig. 5d-j), some degree of coarsening of the α laths is the β grains is observed while the analysis shows that up to this range of temperatures martensitic areas (an example of which is indicated by a white star) remain fundamentally unchanged. Coarsening of the α structure becomes however noticeable and significant at temperatures in excess of 750°C (Figure j-o) as also indicated by high-temperature EBSD analysis (Supplementary Figure S2). Consistently to our HEXRD observations, it is observed a progressive phase transformation that consumes the β matrix. Notably, at temperatures in excess of ~ 800°C, it becomes less obvious to discern the fusion lines of the melt pool boundaries, indicating the range of temperatures needed to completely eliminate the microstructural signature imparted by the PBF-LB. As the temperature further increases, noteworthy are a significant coarsening of grain boundary α and a progressive uniform dissolution of inter-granular α (Fig. 5k-o). Supplementary S2 shows the progressive dissolution of the α and β phase maps obtained in a temperature range comprised between

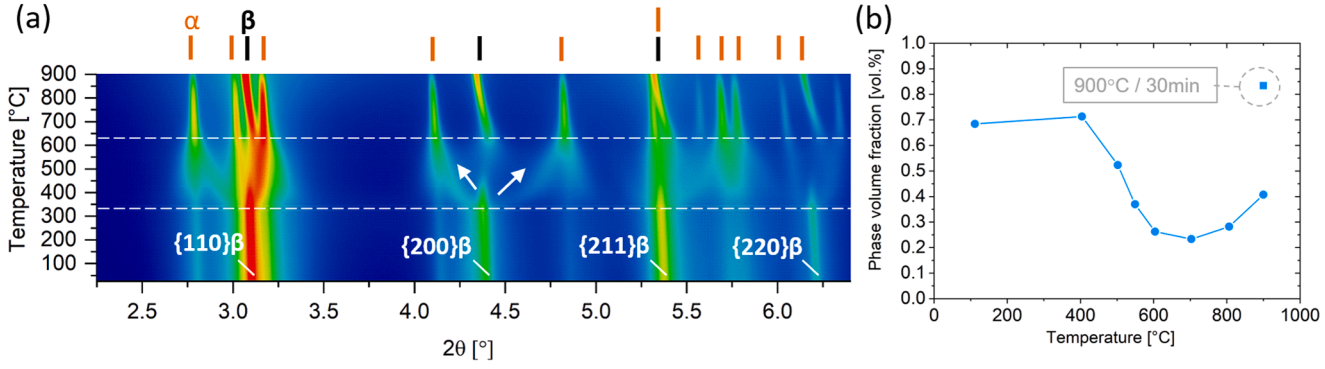

Fig. 4. (a) Color-coded 2D plot corresponding to the evolution of {hkl} reflections during continuous heating of the PBF-LB as-built Ti-6Al-4V-3Fe alloy at 100°C/min from room temperature up to 900°C (α and β reflections are indicated by orange and black markers, respectively) . (b) Evolution of the volume fraction of β as a function of temperature during continuous heating at 100°C. The volume fraction of this phase obtained by Rietveld refinement after annealing at 900°C during 30min is also indicated by a dotted circle.

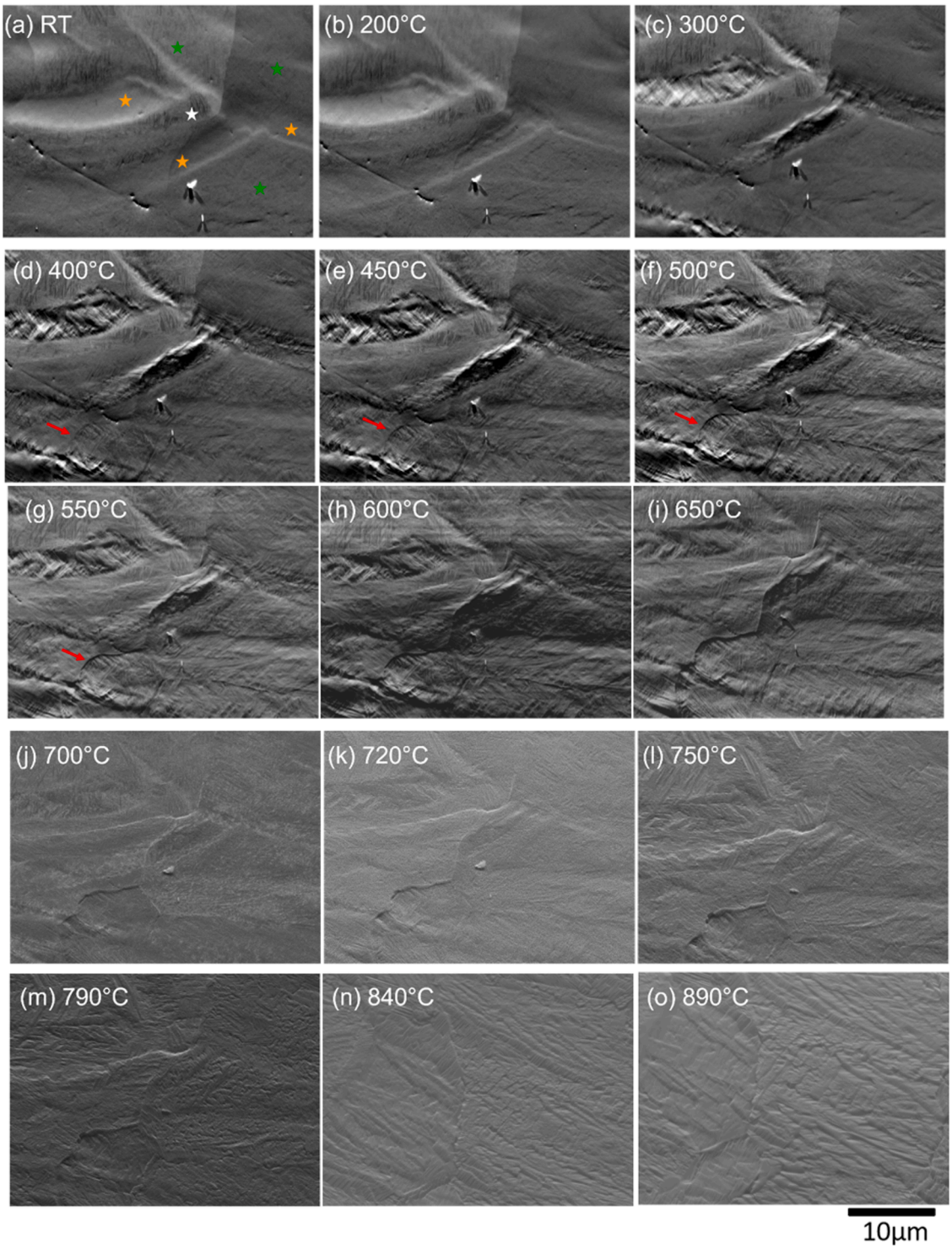

Fig. 5. High temperature in-situ microscopy showing the microstructure evolution of Ti-6Al-4V-3Fe. The micrographs show the same area of interest as the temperature is increased. The temperature at which microscopy is conducted is shown in the top left corner of the micrographs. The green star marker indicates β phase with relative low Fe concentration (these areas are referred to β^{L}). Orange star markers indicate β grains with high concentration of Fe (β^{H}). The white star indicate an example of a martensitic area found in the structure, while red arrows highlight grain boundary α.

720 and 890°C. Moreover, Supplementary S3 shows that a distinct faceted topography is observed on the samples in correspondence of the areas where the α ⇔ β has taken place. The morphological arrangement of these facets finds correspondence to underlying crystal orientation, i.e. facets with identical morphology denote areas with similar texture (Supplementary S3).

As temperature is further increased to 900°C, most of the structure transforms into β phase (Fig. 6). Grain boundary α decorates the boundaries of the β phase pinning its growth. Fig. 6 also shows a significant variation of the grain morphology observed in the top few layers of the build and the rest of the microstructure. Although rejection of Fe during dendritic growth promotes refinement of the β grain structure in the last deposited layer, the addition of new layers causes re-melting of such grains leading to the development of columnar grain morphologies

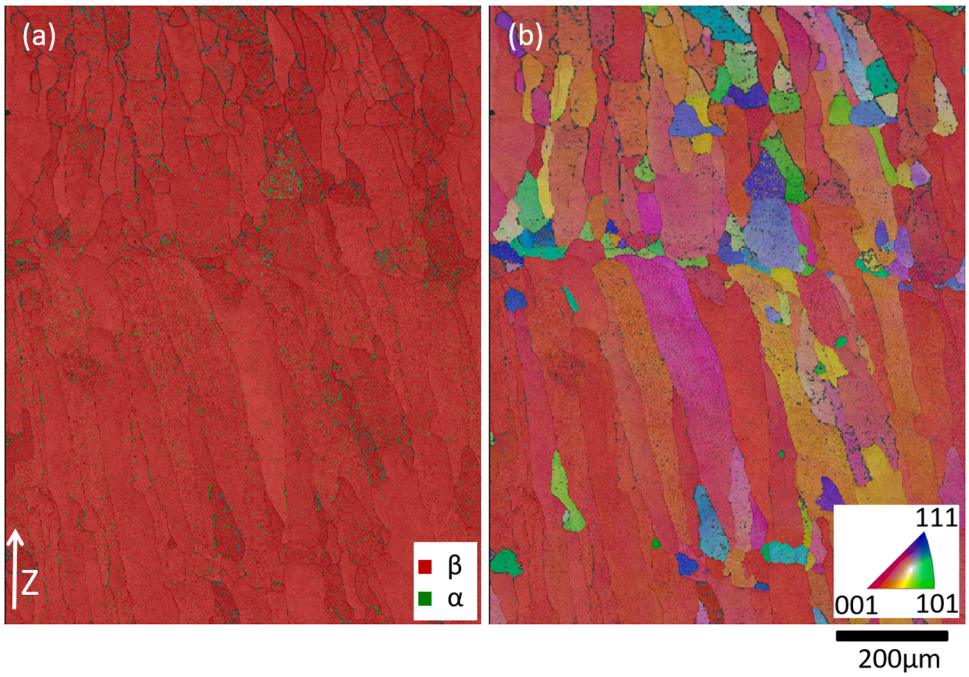

Fig. 6. Microstructural detail of PBF-LB Ti-6Al-4V-3Fe at 900°C. (a) EBSD phase map, β phase mapped in red and α phase mapped in green. The build direction (z) is also indicated; (b) Z-IPF map of the β phase showing significant grain structure evolution in the top portion of the microstructure.

with relative strong <001> crystallographic texture.

3.3. *Ultra-fine microstructures obtained after heat treatment informed by high-temperature microscopy*

On the basis of the kinetic and microstructure analysis obtained in the previous section and to improve the mechanical properties, it was decided to investigate the microstructure evolution of Ti-6Al-4V (reference material) and Ti-6Al-4V-3Fe following heat treatments at temperatures in a range of 700°C to 750°C. Under such heat treatment condition, an effective stress relaxation, significant homogenisation and a fine microstructure could be achieved. The microstructures of Ti-6Al-4V and Ti-6Al-4V-3Fe following the heat treatment at 730°C are compared in Fig. 7. The treatment in Ti-6Al-4V is applied to the α+β field in a relatively low portion of the phase diagram. This causes partial recovery of the microstructure. The α laths have progressively coarsened (lath thickness 0.98 ± 0.08 μm) and are interlaced by thin β phase (showing with bright contrast in Fig. 7a). Thermodynamic calculations indicate that the volume fraction of β phase at 730°C is ~ 5%, a similar β phase fraction at room temperature. On the other hand, Ti-6Al-4V-3Fe shows radically different microstructures (Fig. 7b). Consistently to that observed in the previous section, it is noticed that the interior of the metastable β phase evolves into an ultrafine laminar α+β microstructure (average α lath thickness 0.45 ± 0.04 μm). The prior-β grain boundaries are well delineated by grain boundary α. As expected from sub-transus heat treatments conducted near equilibrium, no morphological changes of the prior-β grains are observed in both alloys [33]. Isolated α-rich regions (also visible in the as-built microstructure) remain discernible in the microstructure: these are indicated by white arrows in Fig. 7b. The measured volume fraction of equilibrium β phase is ~25%

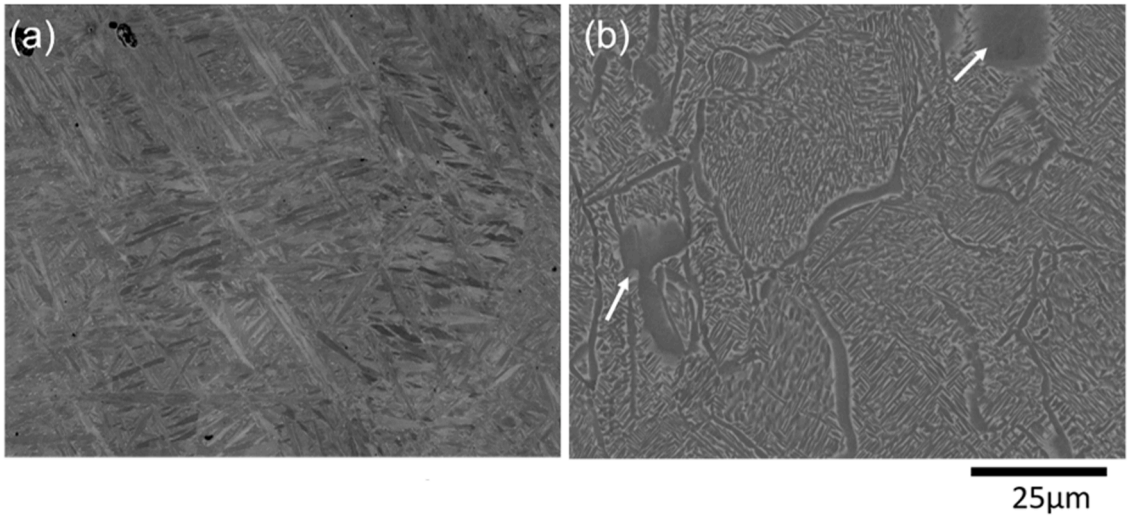

Fig. 7. SEM-BSE images for the microstructures of (a) Ti-6Al-4V and (b) Ti-6Al-4V-Fe obtained after thermal treatment at 730°C during 2h followed by furnace cooling. White arrows indicate martensitic areas lean in Fe.

(reduced from 70% in the as-built condition) indicating strong partition of Fe, a known β stabiliser. As shown in Supplementary Figure S4, perhaps the most striking difference to the microstructure of the reference Ti-6Al-4V is however the fact that α laths within prior- β grains are arranged in colonies of identical texture. Overall, the pole figures show a weak texture, with intensity approx. 7 times the random texture which is comparable to that observed in printed Ti-6Al-4V in the literature [1]. This appear to be the result of the small sized colony microstructure formed within the refined prior- β grains. Apart the arrangement of the α laths (basketweave in Ti-6Al-4V and as colony in Ti-6Al-4V-3Fe), texture analysis reveals no other fundamental differences in the two materials.

The heat treatment improves microstructural uniformity and elemental distribution as also confirmed in Fig. 8. A pronounced element-partitioning is observed. Compared with as-built status (Table 2), high concentration of V and Fe have been observed in the β phase after the heat treatment (Table 3), while Al partitions in the α phase. This is due to the diffusion of both β stabiliser (V, Fe) and α stabiliser (Al) during the near-equilibrium thermal treatment [33].

3.4. Tensile properties of ultra-fine Ti-6Al-4V-3Fe microstructures

The stress-strain curves of all the conducted tensile tests are displayed in Fig. 9, while the corresponding tensile test results after heat treatments in different test directions are summarised in Table 4.

No significant difference is observed in the elastic modulus of the materials, which may link to the dominant hcp α structure present in each microstructure [24]. Meantime, notable discrepancies can be observed in the yield onset and the following plastic deformation of the materials. Compared to Ti-6Al-4V, the heat-treated PBF-LB Ti-6Al-4V-3Fe present a significantly higher strength, both in yield stress and ultimate tensile stress (UTS), as well as a superior ductility.

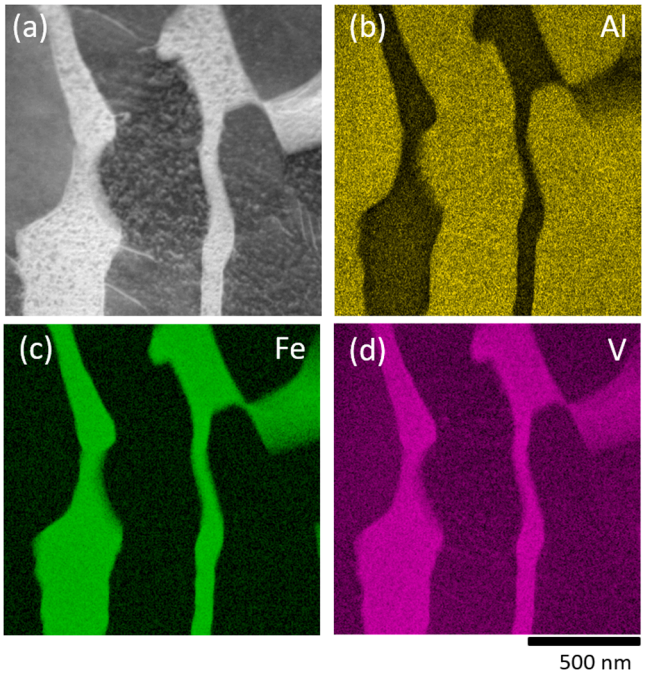

Fig. 8. Microstructure of Ti-6Al-4V-3Fe furnace cooled from 730°C. (a) STEM Bright field image showing the laminar arrangement of the alpha and the β phase. (b), (c), (d) corresponding STEM-EDX maps showing the distribution of aluminium, iron and vanadium, respectively.

Table 3
Composition of Ti-6Al-4V-3Fe after heat treatment at 730°C measured by STEM-EDS.

Microstructural Feature	Element (wt%)			
	Ti	Al	V	Fe
β	bal.	4.1 ± 0.1	9.0 ± 0.1	9.7 ± 0.1
α	bal.	8.3 ± 0.1	1.7 ± 0.1	0.1 ± 0.1

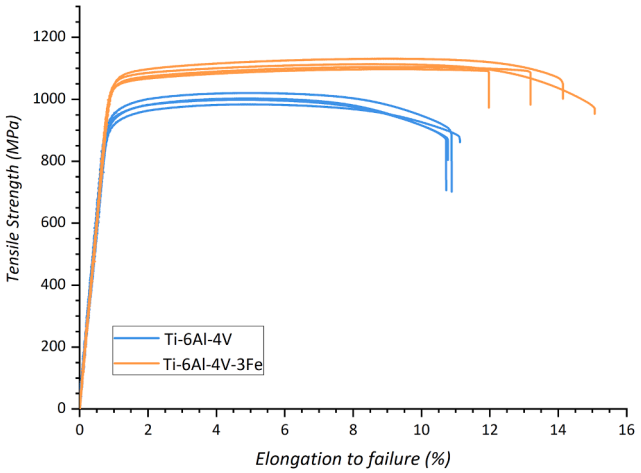

Fig. 9. Engineering stress-strain curves of PBF-LB Ti-6Al-4V and Ti-6Al-4V-3Fe after heat treatment at 730°C followed by furnace cooling

Table 4
Mechanical properties of PBF-LB Ti-6Al-4V and Ti-6Al-4V-3Fe after heat treatment at 730°C followed by furnace cooling.

	Young's modulus E (GPa)	Yield stress σy (MPa)	UTS (MPa)	Elongation ε (%)
Ti-6Al-4V	114 ± 3	936 ± 16	1001 ± 15	10.9 ± 0.2
Ti-6Al-4V -3Fe	118 ± 3	1051 ± 10	1112 ± 14	13.6 ± 1.3

4. Discussion

4.1. Formation of the metastable microstructure in the PBF-LB as-built condition

Although overall approx. 70% of the Ti-6Al-4V-3Fe microstructure constitutes of metastable β, it is clear that the as-built microstructure has no Fe concentration uniformity (Supplementary S1). While it is known that Fe is a potent β stabiliser (approximately 3.5wt% additions in pure Ti lead to the retention of metastable β upon water quenching [34], it is not trivial to determine the precise amounts of Fe that could retain metastable β in the examined quaternary system during PBF-LB. Two factors need to be accounted for. Firstly, the experiments conducted in the study involved the use of non-homogenous powder mixtures. As the mixing of the alloy constituents relies on atomic mixing of the elements in the melt pool and Marangoni flows it results that Fe concentration is generally only uniform within melt pools and concentration non-uniformities arise across different locations in the layers. This can be understood considering that, under analogous processing conditions, melt pool size is only about 500μm length and 300 μm wide with residence times in the liquid state inferior to 1 ms [35]. Secondly, the material is processed with a relatively low volumetric energy density Ev=66.67 J/mm^3, and therefore the limited intrinsic heat input associated to the deposition of adjacent tracks and layers is not sufficient to

generate significant to diffusion-based solid phase transformations in the heat affected zone [7].

4.2. Formation of α from metastable β during heat treatment

The decomposition of metastable β can be interpreted considering the microstructure evolution as the temperature is progressively increased. The formation of the fine α′ structure is observed in the present material in Fig. 2 and Fig. 5. The nucleation of α from β^H (~3.5wt% Fe content) regions of the microstructure at relative low temperatures, is conducible to the intra-granular precipitation of α, which is often observed in metastable β alloys [36]. Non-classical nucleation mechanisms have been proposed to explain the origins of the fine α structure in similar metastable alloys. In most titanium metastable alloys, precipitation is thought to result from heterogenous nucleation of the α phase from nano-scale structures lean in β stabilisers, namely isothermal ω or O″ precipitates, which are uniformly distributed in the interiors of the metastable β grains [2,37,38]. Additionally, alloys where, at a given critical temperature T, the nominal composition of the parent β phase is close (i.e. ~2 wt% of Fe) to c_0(T) (the concentration at which the free energy curves of the parent β and product α phases intersect), might promote intra-granular nucleation of α phase by a pseudo-spinodal transformation [36]. In this case, precipitation is thought to originate in regions of the β grains that experience fluctuation in the composition across c_0, leading to cases where the Gibbs free energy of the product phase (α) is lower than that of the parent phase (β) and thus enabling homogenous decomposition of β [36]. Finally, one should consider the case where pseudo-spinodal transformations are enabled via precursory transformations, such as in alloys which present miscibility gaps to create solute rich and lean regions in the β phase, e.g. in the case of Ti-Mo, Ti-V, Ti-Cr, etc.) [39]. It is thought that such miscibility gap would cause the formation of solute-rich and solute-lean β regions, and in the case where the composition of the latter approaches c_0, pseudo-spinodal transformations might then take place. Nevertheless, as the alloy examined in the study does not present any known miscibility gap in the equilibrium β phase (nor the Ti-Fe and Ti-V binary systems for concentrations of solute similar to that used in the present study), precursory transformations will be not considered in the remainder of the discussion.

As no changes in lattice parameter for temperatures lower than 400°C are observed (Fig. 4), no significant diffusion of the solute is expected to take place during this initial heating stage. This is also supporting by the fact that the diffusivities of the solutes in the in the β phase at temperatures lower than 400°C are negligible. As pseudo-spinodal transformations are congruent, α phase could indeed, at least in principle, form with composition identical to precursor β domain. A fundamental requirement is however the composition of the β grains to be close to c_0(T). Applied the methodology illustrated by S. Nag et al. [36], one can approximate the Gibbs free energies of the two phases (α and β) as a function of composition and temperature using binary phase diagrams (calculated for Mo-equivalency values corresponding to the composition of the alloy). This is shown in Supplementary Figure S5. For example, as the free energy cross over point c_0 at 400°C is expected for alloys with Mo- equivalency values in excess of 26, which would require Fe concentrations in the current alloy in excess of 10 wt.% - which are never observed experimentally. This indicates that pseudo-spinodal decomposition of the β phase is therefore unlikely to take place for temperature below 400°C. A more plausible mechanism for the precipitation of α during low temperature heat treatment (below 400°C) is via heterogenous nucleation on pre-existing athermal ω formed during P-LBF process, which is observed in Fig. 2, or any iso-thermal ω phase that would form as the specimens are heat treated below 400°C. The role of ω in the nucleation of α would also explain the evidence that β^H (regions of higher Fe concentration)– and therefore where one would expect the β to be more stable –are the first to transform upon heating. Indeed, empirical evidence on Ti-Fe binary suggests that a Fe content in excess of 3 wt% is needed to form ω from β-quenching, so it is plausible that nucleation of α via ω precipitates occurs in Fe-rich regions in the build [34]. As the temperature is increased above 450 - 500°C, ω phase is thought to approach its solvus temperature [34]. The shifts of the β peaks observed during HEXRD suggest that Fe diffusion is enabled at relatively low temperatures. It is useful compare the diffusivities of alloying elements in the β phase of titanium using the Arrhenius equation, calculated diffusivities are reported in Table 5 and summarised in Fig. 10. It can be noticed that Fe has a markedly higher diffusivity than V (and Al) in the temperature range 450 to 650°C supporting our high temperature XRD and EBSD observations.

We observe that the interior of the β^L structure is progressively consumed by the α phase and precipitation of grain boundary α along β-grain boundary starts to be discerned. Diffusion of Fe, even at relatively low temperatures (450 to 650°C), could thus enable the α which nucleated on ω precipitates in β^H (or already existing in the matrix as form of nm scale precipitates shown in Fig. 2) to grow by a movement of the α/β interface. The region next to the α is enriched in Fe, i.e. Fe will partition to the β phase during α growth. As α phase is homogeneously distributed in the prior-β grains, the resulting microstructure of α is extremely fine. It is observed that most of the structure consists of α phase with basketweave arrangement at temperatures ~ 700°C (Supplementary Figure S6).

Above 700°C, α to β phase transformation is activated and becomes dominant as the temperature increases, that is the α phase is progressively consumed by the β phase. It is thought that at such high temperatures, the phase transformation is governed primarily by the diffusion of V across the interface as Fe has already partitioned to the β phase. Fig. 11 shows the comparison of the calculated equilibrium phase fractions of Ti-6Al-4V-3Fe at different temperatures with the phase fractions measured experimentally by high-temperature EBSD. The analysis reveals very good agreement particularly at temperatures ~850°C where the α and β phase have grown to equal volume fractions and are well indexed by EBSD. The experimental measured α phase fractions, which is (1- β) have not been shown in Fig. 11 to enhance the clarity and trend of the curve.

4.3. Tensile strength and enhanced ductility in ultra-fine microstructures

Strength in fine lamellar α + β microstructures is typically modelled considering Hall–Petch relationships [11,15] and it is generally accepted that strength increases linearly with the inverse square root of α lath thickness. Fig. 12 summarises data from recent reports [11,24,40-47] on additively manufactured Ti-6Al-4V for which α phase exhibiting a basketweave microstructure. It is interesting to notice that despite the microstructure of Ti-6Al-4V-3Fe after heat-treatment no longer presents a basketweave arrangement, it still shows good agreement with the trend calculated from the literature. It is clear that the reduced α lath size in Ti-6Al-4V-3Fe (estimated at ~400 nm as opposed to 0.98 ± 0.08 μm in Ti-6Al-4V) increases the area fraction of grain boundary and offers significant grain boundary hardening, despite the overall arrangement (basketweave or colony). To evaluate the influence of Fe on the amount of retained room temperature β phase (~25% as opposed to 5% of Ti-6Al-4V) and solid solution strengthening effect on both α and β phases, one can assume that all phases are strained equally and solid solution strengthening from the two phases is analysed with a

Table 5
Coefficients for diffusion in the Ti β phase calculated using Arrhenius equation $D(T) = D_0 \exp(-Q / (R\,T))$.

Element	D_0 [μm²/s]	Q/R [K]
Ti	20000	15000
V	100000	17460
Al	120000	18040
Fe	200000	20712

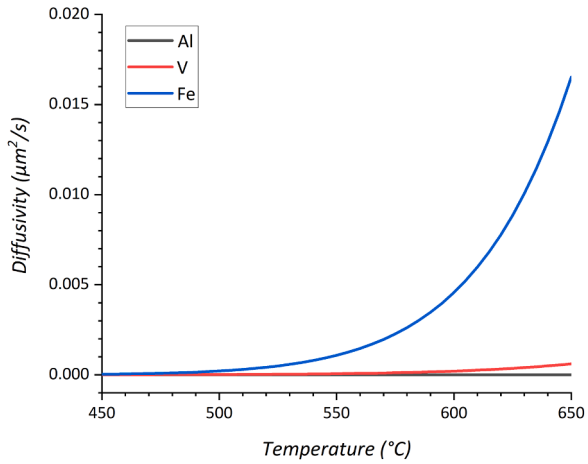

Fig. 10. Estimated diffusivity of solutes in the Ti β phase in the range of temperatures investigated in this study.

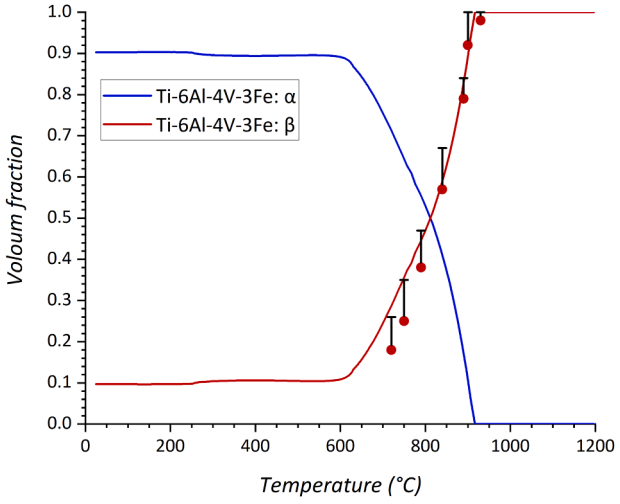

Fig. 11. Equilibrium phase fraction calculated in the Ti-6Al-4V-3Fe system (solid lines) overlaid with phase fraction of β measured by high-temperature EBSD (available for temperatures in excess of 700°C). Portion in the micrograph that are not indexable by EBSD (zero solutions) are reported as uncertainty bars. These are likely to come from the finely distributed phase, i.e. β phase in the temperature range comprised between 700 and 800°C and a phase when temperature approaches β transus temperature.

simple rule of mixtures approach [40,48]. An increase in volume fraction of β phase in Ti-6Al-4V would lead to an inevitable decrease in the overall strength of the alloy as the β phase is the soft phase. Using the model proposed by [40], assuming unchanged Hall-Petch strengthening, retaining 25% of β phase in Ti-6Al-4V would cause a reduction in solid solution strengthening by ~15%. However, after heat treatment at 730°C, Fe partitions almost exclusively in the β phases leading to a significant strengthening of this phase and hence the overall material's strength. As part of future research, the influence of grain boundary α on mechanical anisotropy will be investigated.

Significant improvement in ductility has been observed in Ti-6Al-4V-3Fe compared to its counterpart Ti-6Al-4V. As reported in the literature, the ultrafine lamellar α+β microstructures can evade the general trade off relationship between strength and ductility [40,48] and this offers an explanation for the enhanced ductility of heat treated Ti-6Al-4V-3Fe. Perhaps of even more significance is the consideration of how stress might partition in the two phases: Ti-6Al-4V presents an undesirable arrangement of nm-thin β ribs decorating α laths similar to the as-built

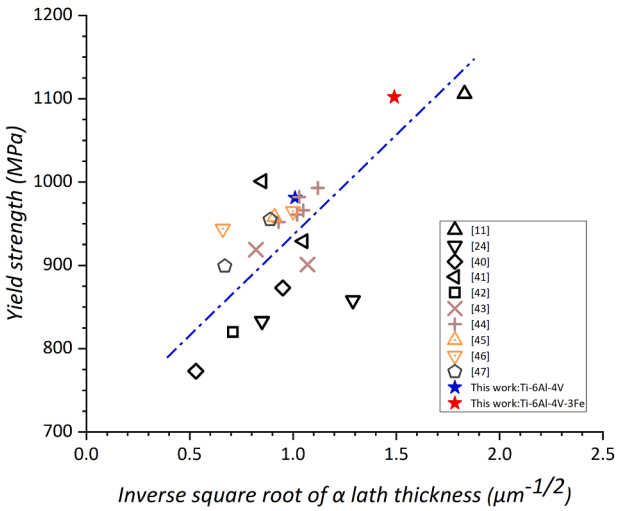

Fig. 12. Dependence of yield strength on the inverse square root of α lath thickness for lamellar α + β microstructures organised with a basketweave arrangement (literature and this study) [11,24,40-47].

microstructure (Fig. 7a) leading to the concentration of stress at the interface of the two phases. The significant amount (25% vs 4% in Ti-6Al-4V) of retained β phase in Ti-6Al-4V-3Fe (Fig. 7b) on the other hand, offers additional opportunities for dislocation slip and would also reduce any stress partitioning effects with positive influence on the material's ductility [49].

5. Conclusions

The combined use of *in-situ* HEXRD and high-temperature microscopy has revealed details of the metastable β decomposition process that occurs in an PBF-LB-fabricated Ti-6Al-4V-3Fe novel quaternary alloy. The main findings are summarised below:

- moderate additions of Fe (up 3 wt. %) to the Ti-6Al-4V have a profound influence on the microstructural development during PBF-LB. Up to 70% metastable β phase is observed in the as-printed samples;
- The local concentration of Fe affects the fraction of the precipitates in the β phase: α′ and athermal ω precipitates are found in iron-rich regions (with a typical Fe concentration exceeding 3.5 wt.%) while iron-lean regions (with Fe concentration only reaching 0.5%) are dominated by α′ martensite;
- The metastable β phase undergoes a significant transformation during heat treatment with distinctive β to α phase transformations taking place between 400 and 650°C; a progressive contraction in the β lattice between 400 and 650°C is attributed to the combined effect of Fe partitioning and overall decrease β volume fraction;
- This is corroborated by high-temperature microscopy which clearly shows homogeneous decomposition of the iron-rich β phase between 400 and 650°C: this transformation is thought to be the result of nucleation of α assisted by the presence of ω phase followed by α phase growth enabled by early diffusion of Fe in the β phase;
- Above 700°C, Ti-6Al-4V-3Fe adopts a conventional phase transformation pathway characterised by the progressive dissolution of α phase via diffusion of V in the β phase: we observe a very good match between high-temperature microscopy investigations and equilibrium phase calculations;
- While heat treatment at intermediate temperature (730°C) enables a partial recovery of the microstructure in Ti-6Al-4V, the same heat treatment enables the attainment of ultrafine α+β microstructures (average α lath thickness 0.45 ± 0.04 μm) in the novel quaternary alloy investigated in this study;

- The ultrafine α+β microstructure developed in this work exhibits an exceptional combination of strength and ductility. The partitioning of Fe in the β phase is thought to be crucial to the attainment of these properties. Firstly, Fe is responsible for the homogeneous decomposition that leads to ultrafine laths that offer significant grain boundary induced hardening (strength is found to correlate well with the inverse square root of the lath thickness). Secondly, its partitioning to the β phase causes marked solid solution strengthening and thus the creation of a "hard" matrix for the α precipitate. Noteworthy is also the fact that the significant amount of β phase after heat treatment might reduce any stress partitioning and enhance the material's ductility.

Declaration of Competing Interest

The authors declare that they have no known competing financial interests or personal relationships that could have appeared to influence the work reported in this paper.

Acknowledgments

The work presented here has been made possible by funding provided through the University of Nottingham's Nottingham Research Fellowship. The authors would like to acknowledge the support provided by Norbert Schell and Andreas Stark (Helmholtz-Zentrum Geesthacht) for the diffraction experiments performed at the P07-HEMS beamline. The Deutsches Elektronen-Synchrotron (DESY) is acknowledged for the provision of synchrotron radiation facilities in the framework of the Proposal I-20210694. P.B.-V. acknowledges financial support from the Spanish Ministry of Science through the Ramón y Cajal grant RYC2020-029585-I. Thanks to Dr Nigel Neate (University of Nottingham) for his assistance on the high temperature microscopy. The authors acknowledge the use of facilities within the Loughborough Materials Characterization Centre.

Supplementary materials

Supplementary material associated with this article can be found, in the online version, at doi:10.1016/j.mtla.2023.101856.

References

[1] S. Liu, Y.C. Shin, Additive manufacturing of Ti6Al4V alloy: A review, Materials & Design 164 (2019), 107552.
[2] Y. Zheng, R.E.A. Williams, D. Wang, R. Shi, S. Nag, P. Kami, J.M. Sosa, R. Banerjee, Y. Wang, H.L. Fraser, Role of ω phase in the formation of extremely refined intragranular α precipitates in metastable β-titanium alloys, Acta Materialia 103 (2016) 850–858.
[3] N.P. Calta, V. Thampy, D.R.C. Lee, A.A. Martin, R. Ganeriwala, J. Wang, P. J. Depond, T.T. Roehling, A.Y. Fong, A.M. Kiss, C.J. Tassone, K.H. Stone, J. Nelson Weker, M.F. Toney, A.W. Van Buuren, M.J. Matthews, Cooling dynamics of two titanium alloys during laser powder bed fusion probed with in situ X-ray imaging and diffraction, Materials & Design 195 (2020), 108987.
[4] S. Hocine, H. Van Swygenhoven, S. Van Petegem, C.S.T. Chang, T. Maimaitiyili, G. Tinti, D.Ferreira Sanchez, D. Grolimund, N. Casati, Operando X-ray diffraction during laser 3D printing, Materials Today 34 (2020) 30–40.
[5] J. Yang, H. Yu, J. Yin, M. Gao, Z. Wang, X. Zeng, Formation and control of martensite in Ti-6Al-4V alloy produced by selective laser melting, Materials & Design 108 (2016) 308–318.
[6] A. Zafari, K. Xia, High Ductility in a fully martensitic microstructure: a paradox in a Ti alloy produced by selective laser melting, Materials Research Letters 6 (11) (2018) 627–633.
[7] J. Haubrich, J. Gussone, P. Barriobero-Vila, P. Kürnsteiner, E.A. Jägle, D. Raabe, N. Schell, G. Requena, The role of lattice defects, element partitioning and intrinsic heat effects on the microstructure in selective laser melted Ti-6Al-4V, Acta Materialia 167 (2019) 136–148.
[8] S.M. Kelly, S.L. Kampe, Microstructural evolution in laser-deposited multilayer Ti-6Al-4V builds: Part II, Thermal modeling, Metall and Mat Trans A 35 (6) (2004) 1869–1879.
[9] P. Barriobero-Vila, J. Gussone, J. Haubrich, S. Sandlöbes, C.J. Da Silva, P. Cloetens, N. Schell, G. Requena, Inducing Stable α + β Microstructures during Selective Laser Melting of Ti-6Al-4V Using Intensified Intrinsic Heat Treatments, Materials 10 (3) (2017).
[10] C. Kenel, D. Grolimund, X. Li, E. Panepucci, V.A. Samson, D.F. Sanchez, F. Marone, C. Leinenbach, In situ investigation of phase transformations in Ti-6Al-4V under additive manufacturing conditions combining laser melting and high-speed micro-X-ray diffraction, Scientific Reports 7 (1) (2017) 16358.
[11] W. Xu, M. Brandt, S. Sun, J. Elambasseril, Q. Liu, K. Latham, K. Xia, M. Qian, Additive manufacturing of strong and ductile Ti–6Al–4V by selective laser melting via in situ martensite decomposition, Acta Materialia 85 (2015) 74–84.
[12] T. Song, T. Dong, S.L. Lu, K. Kondoh, R. Das, M. Brandt, M. Qian, Simulation-informed laser metal powder deposition of Ti-6Al-4V with ultrafine α-β lamellar structures for desired tensile properties, Additive Manufacturing 46 (2021), 102139.
[13] M. Chen, S. Van Petegem, Z. Zou, M. Simonelli, Y.Y. Tse, C.S.T. Chang, M. G. Makowska, D.Ferreira Sanchez, H. Moens-Van Swygenhoven, Microstructural engineering of a dual-phase Ti-Al-V-Fe alloy via in situ alloying during laser powder bed fusion, Additive Manufacturing 59 (2022), 103173.
[14] S. Cao, R. Chu, X. Zhou, K. Yang, Q. Jia, C.V.S. Lim, A. Huang, X. Wu, Role of martensite decomposition in tensile properties of selective laser melted Ti-6Al-4V, Journal of Alloys and Compounds 744 (2018) 357–363.
[15] W. Xu, E.W. Lui, A. Pateras, M. Qian, M. Brandt, In situ tailoring microstructure in additively manufactured Ti-6Al-4V for superior mechanical performance, Acta Materialia 125 (2017) 390–400.
[16] P. Barriobero-Vila, K. Artzt, A. Stark, N. Schell, M. Siggel, J. Gussone, J. Kleinert, W. Kitsche, G. Requena, J. Haubrich, Mapping the geometry of Ti-6Al-4V: From martensite decomposition to localized spheroidization during selective laser melting, Scripta Materialia 182 (2020) 48–52.
[17] M. Laleh, E. Sadeghi, R.I. Revilla, Q. Chao, N. Haghdadi, A.E. Hughes, W. Xu, I. De Graeve, M. Qian, I. Gibson, M.Y. Tan, Heat treatment for metal additive manufacturing, Progress in Materials Science 133 (2023), 101051.
[18] M. Motyka, A. Baran-Sadleja, J. Sieniawski, M. Wierzbinska, K. Gancarczyk, Decomposition of deformed α′(α″) martensitic phase in Ti–6Al–4V alloy, Materials Science and Technology 35 (3) (2019) 260–272.
[19] M. Simonelli, D.G. McCartney, P. Barriobero-Vila, N.T. Aboulkhair, Y.Y. Tse, A. Clare, R. Hague, The Influence of Iron in Minimizing the Microstructural Anisotropy of Ti-6Al-4V Produced by Laser Powder-Bed Fusion, Metall and Mat Trans A 51 (5) (2020) 2444–2459.
[20] B.A. Welk, N. Taylor, Z. Kloenne, K.J. Chaput, S. Fox, H.L. Fraser, Use of Alloying to Effect an Equiaxed Microstructure in Additive Manufacturing and Subsequent Heat Treatment of High-Strength Titanium Alloys, Metall and Mat Trans A 52 (12) (2021) 5367–5380.
[21] M.J. Bermingham, D. Kent, B. Pace, J.M. Cairney, M.S. Dargusch, High strength heat-treatable β-titanium alloy for additive manufacturing, Materials Science and Engineering: A 791 (2020), 139646.
[22] I. ASTM, ASTM E8/E8M-16a: Standard Test Methods for Tension Testing of Metallic Materials, ASTM International, West Conshohocken, PA, USA, 2016.
[23] G.F. Vander Voort, A. Roósz, Measurement of the interlamellar spacing of pearlite, Metallography 17 (1) (1984) 1–17.
[24] Z. Zou, M. Simonelli, J. Katrib, G. Dimitrakis, R. Hague, Microstructure and tensile properties of additive manufactured Ti-6Al-4V with refined prior-β grain structure obtained by rapid heat treatment, Materials Science and Engineering: A 814 (2021), 141271.
[25] P. Barriobero-Vila, J. Gussone, A. Stark, N. Schell, J. Haubrich, G. Requena, Peritectic titanium alloys for 3D printing, Nature Communications 9 (1) (2018) 3426.
[26] L. Lutterotti, S. Matthies, H.R. Wenk, A.S. Schultz, J.W. Richardson, Combined texture and structure analysis of deformed limestone from time-of-flight neutron diffraction spectra, Journal of Applied Physics 81 (2) (1997) 594–600.
[27] A. Idhil Ismail, M. Dehmas, E. Aeby-Gautier, B. Appolaire, In-Situ Investigation of Phase Transformation Kinetics in Ti-6Al-4V Under Rapid Heating Condition Using High-Energy Synchrotron Diffraction, Proceedings of the 13th World Conference on Titanium (2016) 591–598.
[28] G. Lütjering, J.C. Williams, Titanium, Springer Science & Business Media 2007.
[29] I. Polmear, Light alloys: from traditional alloys to nanocrystals, Butterworth-Heinemann, 2005.
[30] B. Vrancken, L. Thijs, J.P. Kruth, J. Van Humbeeck, Microstructure and mechanical properties of a novel β titanium metallic composite by selective laser melting, Acta Materialia 68 (2014) 150–158.
[31] F.F. Ahmed, S.J. Clark, C.L. Alex Leung, L. Stanger, J. Willmott, S. Marussi, V. Honkimaki, N. Haynes, H.S. Zurob, P.D. Lee, A.B. Phillion, Achieving homogeneity in a high-Fe β-Ti alloy laser-printed from blended elemental powders, Materials & Design 210 (2021), 110072.
[32] J.W. Elmer, T.A. Palmer, S.S. Babu, E.D. Specht, In situ observations of lattice expansion and transformation rates of α and β phases in Ti–6Al–4V, Materials Science and Engineering: A 391 (1) (2005) 104–113.
[33] X.-Y. Zhang, G. Fang, S. Leeflang, A.J. Böttger, A. Zadpoor, J. Zhou, Effect of subtransus heat treatment on the microstructure and mechanical properties of additively manufactured Ti-6Al-4V alloy, Journal of Alloys and Compounds 735 (2018) 1562–1575.
[34] J.L. Murray, The Fe−Ti (Iron-Titanium) system, Bulletin of Alloy Phase Diagrams 2 (3) (1981) 320–334.
[35] P.A. Hooper, Melt pool temperature and cooling rates in laser powder bed fusion, Additive Manufacturing 22 (2018) 548–559.
[36] S. Nag, Y. Zheng, R.E.A. Williams, A. Devaraj, A. Boyne, Y. Wang, P.C. Collins, G. B. Viswanathan, J.S. Tiley, B.C. Muddle, R. Banerjee, H.L. Fraser, Non-classical homogeneous precipitation mediated by compositional fluctuations in titanium alloys, Acta Materialia 60 (18) (2012) 6247–6256.

[37] R. Shi, Y. Zheng, R. Banerjee, H.L. Fraser, Y. Wang, ω-Assisted α nucleation in a metastable β titanium alloy, Scripta Materialia 171 (2019) 62–66.
[38] Y. Zheng, S. Antonov, Q. Feng, R. Banerjee, D. Banerjee, H.L. Fraser, Shuffle-induced modulated structure and heating-induced ordering in the metastable β-titanium alloy, Ti-5Al-5Mo-5V-3Cr, Scripta Materialia 176 (2020) 7–11.
[39] T. Zhang, D. Wang, Y. Wang, Novel transformation pathway and heterogeneous precipitate microstructure in Ti-alloys, Acta Materialia 196 (2020) 409–417.
[40] B.J. Hayes, B.W. Martin, B. Welk, S.J. Kuhr, T.K. Ales, D.A. Brice, I. Ghamarian, A. H. Baker, C.V. Haden, D.G. Harlow, H.L. Fraser, P.C. Collins, Predicting tensile properties of Ti-6Al-4V produced via directed energy deposition, Acta Materialia 133 (2017) 120–133.
[41] H. Galarraga, R.J. Warren, D.A. Lados, R.R. Dehoff, M.M. Kirka, P. Nandwana, Effects of heat treatments on microstructure and properties of Ti-6Al-4V ELI alloy fabricated by electron beam melting (EBM), Materials Science and Engineering: A 685 (2017) 417–428.
[42] J.S. Jha, S.P. Toppo, R. Singh, A. Tewari, S.K. Mishra, Deformation behavior of Ti-6Al-4V microstructures under uniaxial loading: Equiaxed Vs. transformed-β microstructures, Materials Characterization 171 (2021), 110780.
[43] S.L. Lu, Z.J. Zhang, R. Liu, X.H. Zhou, X.G. Wang, B.N. Zhang, X.M. Zhao, J. Eckert, Z.F. Zhang, Optimal tensile properties of laser powder bed fusion hereditary basket-weave microstructure in additive manufactured Ti6Al4V, Additive Manufacturing 59 (2022), 103092.
[44] N. Hrabe, T. Quinn, Effects of processing on microstructure and mechanical properties of a titanium alloy (Ti–6Al–4V) fabricated using electron beam melting (EBM), Part 2: Energy input, orientation, and location, Materials Science and Engineering: A 573 (2013) 271–277.
[45] M. Simonelli, Y.Y. Tse, C. Tuck, Effect of the build orientation on the mechanical properties and fracture modes of SLM Ti–6Al–4V, Materials Science and Engineering: A 616 (2014) 1–11.
[46] T. Vilaro, C. Colin, J.D. Bartout, As-Fabricated and Heat-Treated Microstructures of the Ti-6Al-4V Alloy Processed by Selective Laser Melting, Metall and Mat Trans A 42 (10) (2011) 3190–3199.
[47] B. Vrancken, L. Thijs, J.-P. Kruth, J. Van Humbeeck, Heat treatment of Ti6Al4V produced by Selective Laser Melting: Microstructure and mechanical properties, Journal of Alloys and Compounds 541 (2012) 177–185.
[48] X. Yang, R.A. Barrett, N.M. Harrison, S.B. Leen, A physically-based structure-property model for additively manufactured Ti-6Al-4V, Materials & Design 205 (2021), 109709.
[49] D. Zhang, L. Wang, H. Zhang, A. Maldar, G. Zhu, W. Chen, J.-S. Park, J. Wang, X. Zeng, Effect of heat treatment on the tensile behavior of selective laser melted Ti-6Al-4V by in situ X-ray characterization, Acta Materialia 189 (2020) 93–104.